Available online at www.sciencedirect.com
ScienceDirect
Deep-Sea Research I 54 (2007) 856–870
DEEP-SEA RESEARCH PART I
www.elsevier.com/locate/dsri

Inertial and tidal shear variability above Reykjanes Ridge

Hans van Haren*

Royal Netherlands Institute for Sea Research (NIOZ), P.O. Box 59, 1790 AB Den Burg, The Netherlands

Received 18 August 2006; received in revised form 26 February 2007; accepted 9 March 2007
Available online 14 March 2007

Abstract

Yearlong 75 kHz acoustic Doppler current profiler (ADCP) data were obtained well above Reykjanes Ridge (northern extension of the Mid-Atlantic Ridge (MAR)). The area is characterized by relatively large semidiurnal tidal ('D_2') currents that have (at lunar M_2) more than half a decade larger variance than inertial (f) currents. However, despite the relatively weak near-inertial kinetic energy, its vertical current shear shows larger magnitudes than at M_2 in an otherwise flat $f-D_2$ band limited between frequencies 0.74 and 1.35f, which equals the inertio-gravity wave bounds $[\sigma_{\min}, \sigma_{\max}](N=f)$. N represents the buoyancy frequency. The shear in this band dominates all shear computed at 20 m effective vertical scale. As the kinetic energy spectrum peaks at M_2, but not (significantly) at S_2 and N_2, a difference in tidal (and inertial) scales and hence sources is observed. M_2-tides contribute mostly to large-scale coherent motions. The dominant incoherent $f-D_2$ shear is highly variable in time (~2-day periodicity). Furthermore, inertial and tidal shear are more or less completely separated in space and time, each occurring in different layers in the vertical. The thin shear layers reflect the rapidly varying short vertical scale N_s profile, to within the ~20 m limitation of ADCP data, rather than the large-scale smooth N_L. In each of large-N_s layers $Ri \approx 1$, probably. The yearlong smoothed shear magnitude follows N_L, but only as stable $Ri \approx 5$. The shear polarization is more circular than rectilinear, albeit varying with time, and highly symmetric around f. During transitions, e.g., between stratified and homogeneous layers and between waves from varying sources, near-circular motions can generate near-rectilinear shear in the direction of wave propagation (in the direction of the minor axis of the current ellipse). This contrasts with the possibility of near-rectilinear barotropic oscillatory motions generating near-circular shear under viscosity in shallow seas.

Keywords: Internal wave shear; Inertial and tidal dominance; Mid-Atlantic Ridge; 75 kHz ADCP data

1. Introduction

It is well established under the traditional approximation that in a static density (ρ) stratified ocean the internal gravity wave frequency (σ) band is defined $f<\sigma<N=(-g/\rho\,\partial\rho/\partial z-g^2/c_s^2)^{1/2}$, where g denotes the acceleration of gravity, c_s the speed of sound, N the buoyancy frequency $N \ll f = 2\Omega \sin\varphi$, and f the inertial frequency representing the local vertical component of the Earth's rotational vector Ω at latitude φ. Within this band, most kinetic energy E_k is found at low frequencies, very near f (usually 1.00–1.05f, Fu, 1981) and at semidiurnal tidal frequencies ($M_2, S_2, ,\ldots$, henceforth indicated in the text in short notation 'D_2' when no specific, lunar, solar, ,…, harmonic frequency is meant). Energy varies, commonly with N for frequencies

*Tel.: +31 222 369300/369451; fax: +31 222 319674.
E-mail address: hansvh@nioz.nl.

0967-0637/$ - see front matter © 2007 Elsevier Ltd. All rights reserved.
doi:10.1016/j.dsr.2007.03.003

away from the boundaries f and N: $E_k \sim N$, following the internal gravity wave model by Garrett and Munk (1972), and also with location, for example, showing relatively large values over topography (Baines, 1982). Major sources for internal tides are large topographic features such as the top of continental slopes and seamounts. Geostrophic adjustment, for example, following the passage of atmospheric disturbances and fronts, is thought as a major source for inertial internal wave generation (e.g., Davies and Xing, 2005).

Breaking internal waves are considered to be one of the most important mechanisms for diapycnal mixing in the open ocean, with a likely importance for large-scale near-inertial waves in creating critical conditions for diapycnal turbulent mixing induced via shear or convective instability (Turner, 1973; Woods, 1980). As vertical shear is defined by $\mathbf{S} = (\partial u/\partial z, \partial v/\partial z)$ for horizontal current components (u, v) along Cartesian coordinates (x, y), (finite) vertical variations Δz are a key variable for internal-wave-induced mixing. It is expected that largest shear is generated by most energetic motions, at f and D_2. However, the overall picture of internal-wave-induced mixing is still not clear. In particular, long-term observational evidence of typical frequencies and vertical (z) length scales (Δz) that dominate vertical current differences in the ocean have not been presented.

Strong suggestions from microstructure observations have been made for shear roll off at $\Delta z = 10$ m (Gargett et al., 1981), and the same length scale has been suggested for most favored internal waves breaking via convective instability (Orlanski and Bryan, 1969). The shear at this scale seems an adequate parameterization for describing turbulent mixing (Gregg, 1989). Yet, the shear variability with time and its dominant source, be it inertial motions, tides or mesoscale eddies, have not been specified for general open-ocean areas over a prolonged period of time.

This paper presents yearlong finite vertical current difference ('shear') observations obtained using acoustic Doppler current profiler (ADCP) data from mid-depth above the Reykjanes Ridge, the mid-Atlantic Ridge (MAR) extension in the Irminger Sea. This is a rough open-ocean topography above which enhanced mixing is expected (Polzin et al., 1997; Walter et al., 2005). The observed shear is compared with CTD-profile observations of variations in vertical density stratification.

2. Shear and stratification

Several days of profiling observations by Leaman and Sanford (1975) and Leaman (1976) suggested relatively short vertical scales $\Delta z = O(100\,\mathrm{m})$ for *inertial* motions in the ocean. Slightly smaller scales are reported for similar lengths of time series by Alford and Pinkel (2000) and, for 2-week time series, by Pinkel (1983). Alford and Pinkel (2000) documented $O(10$–$100\,\mathrm{m})$ thick layers of shear, computed over 6.4 m vertically, that persist for several hours. This shear was associated with inertial motions, but it is noted that frequencies were not well resolved because of the shortness of records.

Although to my knowledge no similar detailed observational account has been given of the vertical length scales of internal *tidal* waves, investigations from the South-Atlantic MAR suggest that large vertical scales $O(1000\,\mathrm{m})$, 'low modes' 3–5, dominate the energy flux in most areas, except perhaps very near a source, say less than some 10 km away from substantial topography (St. Laurent and Garrett, 2002). However, the same authors show that the energetically weak motions at scales down to $\Delta z \approx 10$ m (vertical modes up to 300) are a prerequisite for the gradient Richardson number $Ri = N^2/|\mathbf{S}|^2 \approx 1$, a necessary condition for destabilizing shear to overcome the stable stratification in a 3-D, non-linear internal wave field (Abarbanel et al., 1984). Such marginal stability conditions $0.25 < Ri < 1$ evidence a liaison between N and $|\mathbf{S}|$, most likely at f, D_2 as has been observed in strongly stratified shelf seas (van Haren et al., 1999).

Hence, questions arise as to where all this inertial/tidal energy is dissipated or absorbed in the deep ocean and how it attains its small vertical scale. Higher modes (small vertical length scales) may be simply a consequence of internal (tidal) wave generation at a spatially limited topographic source, so that energy propagates away in beams. Also for the ocean interior, Orlanski and Bryan (1969) modeled small-scale internal waves from non-linear interaction between waves from multiple sources. Whatever the generation, this vertical scale Δz seems to be associated with shear or convective instabilities, diapycnal mixing and, thus, changes in stratification.

In general, large-scale $N = N_L$ is assumed to vary on relatively slow sub-inertial time scales. However, straining of isopycnals may cause small-scale variations of N; we therefore denote N with such

variations as N_s, so that one expects Ri to vary around its marginal equilibrium as well. Although f, D_2 shear varies at (super-) inertial scales, the shear *magnitude* (contained in Ri) generally varies at sub-inertial scales (van Haren, 2000). This is because near-circular motions (such as commonly are observed at f, although only in stratified waters (van Haren and Millot, 2004)), create 'constant' $|\mathbf{S}|$, regardless of whether $\mathbf{S}$ is governed by a vertical change in amplitude or in phase. Likewise, at high latitudes free internal D_2 waves have relatively large polarization $e = a/b$, a denoting the minor and b the major ellipse axis, according to the simple model (Gonella, 1972) that $e = f/\sigma = 0.86(S_2) - 0.89(M_2)$ (here $e = 1$ corresponds to circular polarization, $e = 0$ rectilinear polarization). The remaining question is how small vertical scale waves are generated at these frequencies, so that they may cause substantial shear in the context of small Ri.

A recently hypothesized (van Haren and Millot, 2004) possibility is a change in (near-inertial) propagation properties when waves pass from stratified to homogeneous layers, with near-circular inertial motions and shear in stratified layers and more rectilinear polarization in homogeneous layers. This implies the largest $|\mathbf{S}|$ and lowest Ri in layers of high N_s, as has been suggested for upper-ocean shear and strain by Pinkel and Anderson (1997). This is pursued further here for the ocean interior by investigating the dominant shear frequencies and vertical scales above the MAR. These observations may be useful for modeling internal wave shear and associated mixing.

3. Data

An upward looking 75 kHz RDI-ADCP was mounted in the topbuoy of a mooring located in ~1550 m water depth just west of the crest of the Reykjanes Ridge (Fig. 1) between August 2003 and October 2004 (see Table 1 for details). The ADCP was set to range ~655 m from the head, or ~40% of the water column around mid-depth. A substantial part (between 420 and 1020 m) of the range returned permanently good data, presumably due to large amounts of scatterers. The rest of the range near the edges showed bad data mainly between days 350 and 450 (in winter), except for yearlong poor data return in the lower 20 m near the ADCP, possibly due to the recovery line and float.

Pressure and tilt sensor information showed that the mooring did not move much (Fig. 2), $<1.2^\circ$ tilt angle implying <0.12 m motion in z and <11 m in x, y, due to the use of a large, elliptically shaped, low-drag buoyancy element. The pressure sensor data could thus be used as a reasonable representative of tidal range estimates ($\sim\pm 2$ dbar), after accounting for the slow decrease in pressure by about 0.3 dbar over the full length of the record due to stretching of the steel mooring cable.

SeaBird-911 CTD observations, obtained along a transect perpendicular to the Reykjanes Ridge during the deployment cruise, show considerable variation in stratification across the ADCP's range (Fig. 2d–f). Density variations are dominated by temperature variations, also at the ADCP. There, temperature varies by 1.5 °C over the entire period

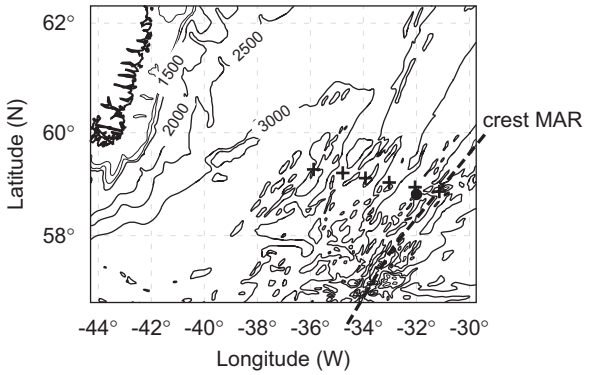

Fig. 1. Mooring position (●) and positions of CTD stations (+) above the Reykjanes Ridge (northern Mid-Atlantic Ridge extension; dashed line indicates the approximate crest location) in the Irminger Sea, East of Greenland (upper-left corner). Depths in m.

Table 1
Upward-looking ADCP mooring details

Latitude	58°48.72′N
Longitude	031°59.80′W
Water depth	1550 m
f, period T_f	1.7150 cpd, 14.0 h
Deployment	26 August 2003
Recovery	07 October 2004
RDI 75 kHz ADCP	Longranger
Beam slant angle	20°
Transmission length	15 m
Instrument depth	1040 m
First bin	1026 m
# Bins × bin size	80 × 8 m
Ensemble period	900 s
Local stratification, N	31 ± 5 cpd
Std u, v	0.03 m s^{-1}/ens
Std w	0.01 m s^{-1}/ens

Frequency is in cycles per day (1 cpd = $2\pi/86\,400$ s^{-1}).

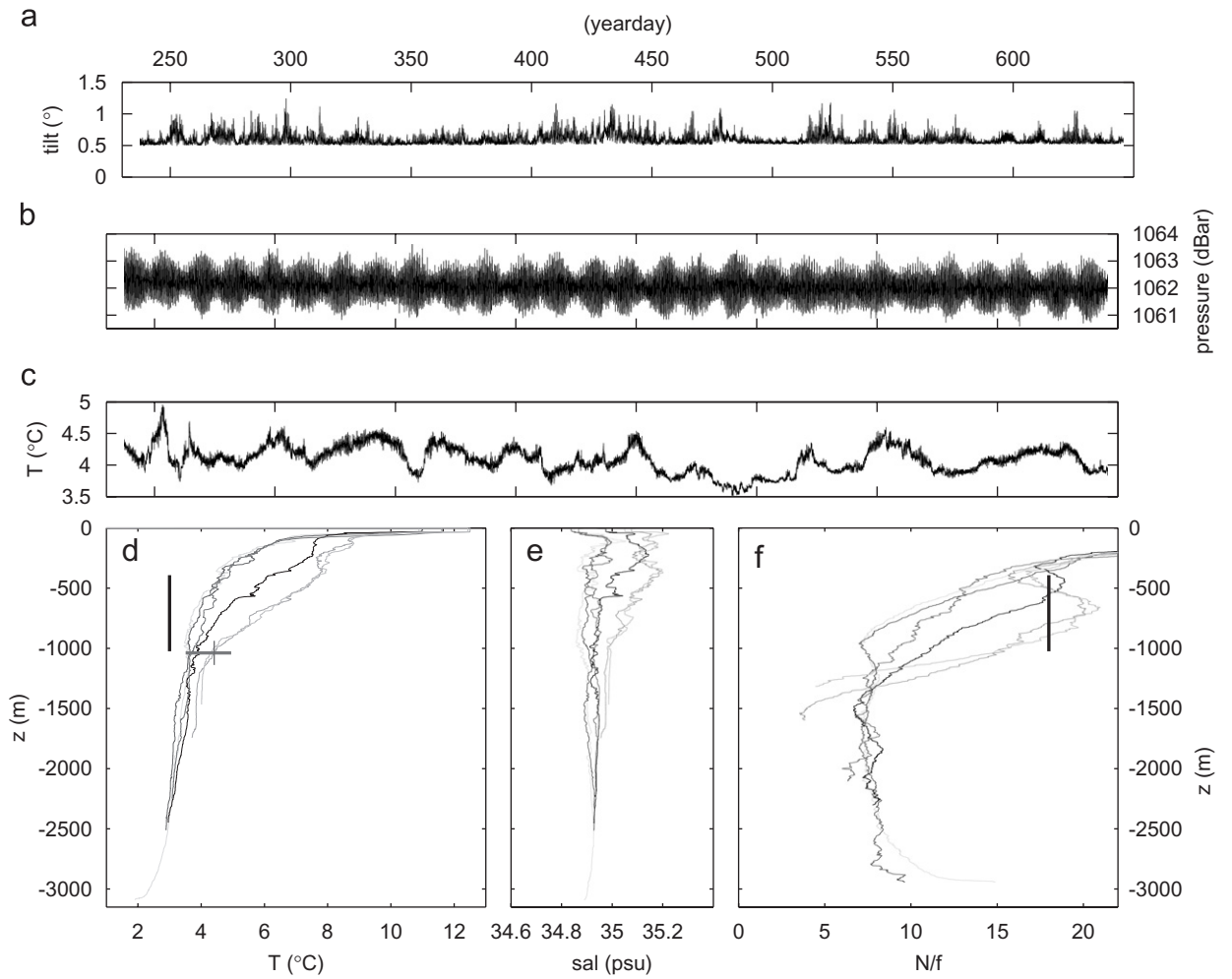

Fig. 2. (a) Yearlong time series of ADCP's tilt; (b) pressure; (c) temperature. Yeardays in 2004 are +365; (d) profiles with depth of temperature measured at 6 CTD stations (Fig. 1) down the Reykjanes Ridge. The vertical bar indicates the ADCP range, the horizontal red bar the ADCP's temperature range and the thin vertical blue line the ADCP's temperature at the start of the record ≈ time of CTD, (e) profiles of salinity; (f) profiles of stratification computed over $\Delta z = 300$ m. The black vertical bar indicates the same z-range as in (d).

(Fig. 2c), with occasional strong decreases associated with horizontal (frontal) advection, or, when they occur in winter, associated with deep convection. Salinity contribution to density variations is small, and weakly favorable for double-diffusive mixing in the ADCP range. The variation in stratification is observed at the large scale using $\Delta z = 300$ m to compute $N_L = 18 \pm 3f$, and also on the smaller scale using $\Delta z = 8$ m, giving $N_s = 18 \pm 10f$ (Fig. 3). In the latter, three occurrences of $N = 0$ are observed in the ADCP range. Note that for the latter computation the portion of instrumental error contributing to the uncertainty in N is still only $\pm 2f$, so that the remainder is attributable to environmental variability. The scale $\Delta z = 8$ m equals the vertical bin size of the ADCP (Table 1), but due to the larger transmission length (~15 m) of the triangularly shaped and 15% overlapping acoustic pulses, statistically independent estimates are expected across vertical distances of ~18 m.

An overview of the raw data demonstrates the variability with time as well as the relative importance of short-periodic (f, D_2) motions (Fig. 4). Because of the specific set-up of an upward looking instrument towards the larger stratification of the quasi-permanent pycnocline (Fig. 2) and towards the larger sub-inertial currents, the highest signal-to-noise ratio (s/n) is not found close to the instrument, as is most common. This is also due to the larger number of zooplankton near and above

the pycnocline, as inferred from the diurnal migration pattern found in w-data above 600 m (not shown). This vertical s/n distribution favors the extent of good data over nearly the entire ADCP range.

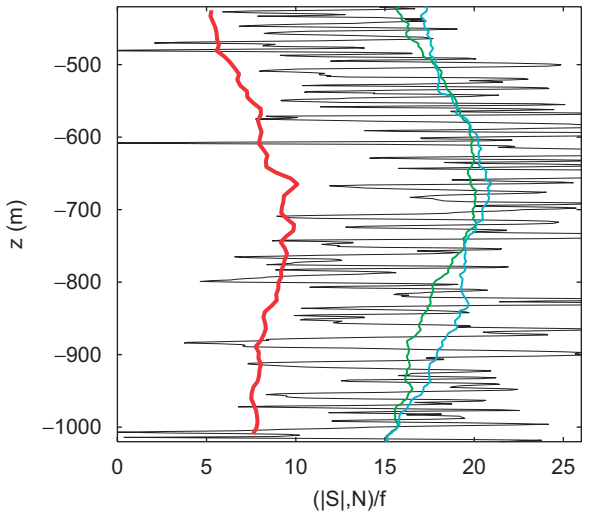

Fig. 3. Stratification computed from CTD data over $\Delta z = 300$ m (light blue and, from a nearby station, green, cf. profiles in Fig. 2) and $\Delta p = 9$ dbar (thin black). In red the yearlong mean near inertial and semidiurnal tidal shear ($\Delta z = 8$ m).

Kinetic energy spectra confirm that motions in the area are dominated at D_2, followed by low frequency ($\sigma < 0.1$ cpd) and f-motions (Fig. 5). The tidal motions are quite rectilinear, $e \approx 0.1$–0.2, therefore mostly constituting barotropic or large-scale (coherent) baroclinic motions (Fig. 5b). The remainder of a typical yearlong polarization spectrum follows linear internal wave theory for frequencies $f < \sigma \sim < 4$ cpd. However, the smooth spectra virtually do not show higher harmonics except for some small, statistically barely significant peaks at $M_2 + f$, M_4. Although modeling studies (e.g., Davies and Xing, 2003) demonstrate different mechanisms that generate motions at these interaction frequencies, these motions appear here as one in a single-frequency band. At higher frequencies instrumental noise becomes increasingly more important in ADCP's u, v data.

Comparison with data from a single-point mechanical (Valeport BFM-308) current meter at ~1000 m in a mooring 35 km to the east shows that the ADCP's E_k-spectra are significantly different from the better resolved Valeport spectrum for $\sigma > \sim 7$ cpd (Fig. 5a). This is also noticeable in the rotary spectra (Fig. 5b), where the Valeport data show larger polarization than the ADCP data for $\sigma > \sim 1$ cpd ($0.6f$). Nevertheless, both data sets show

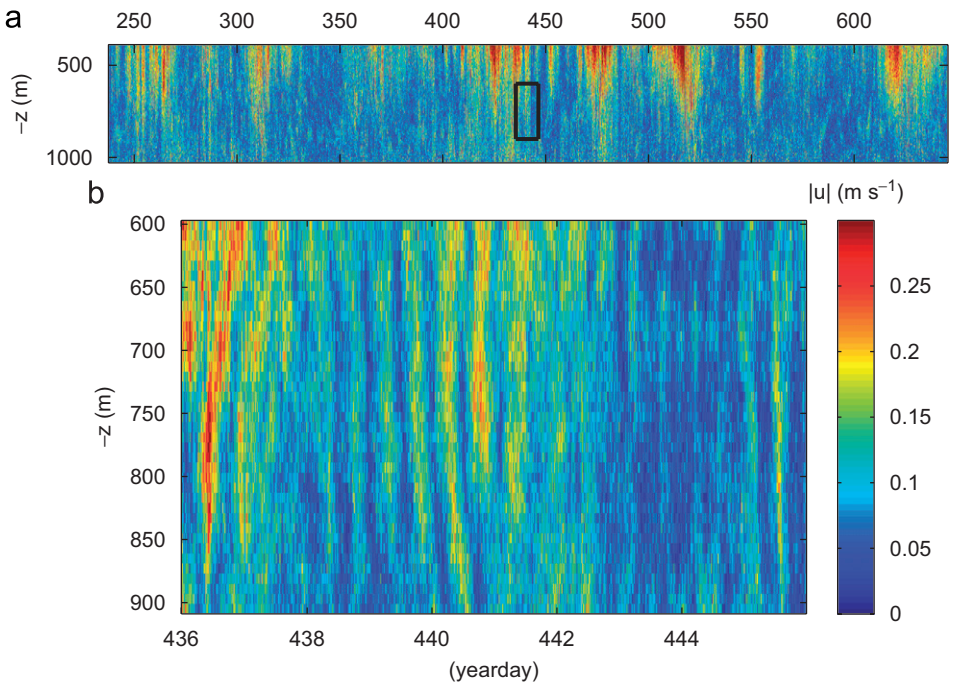

Fig. 4. (a) Yearlong depth time series of raw total current amplitude. (b) Detail of a.

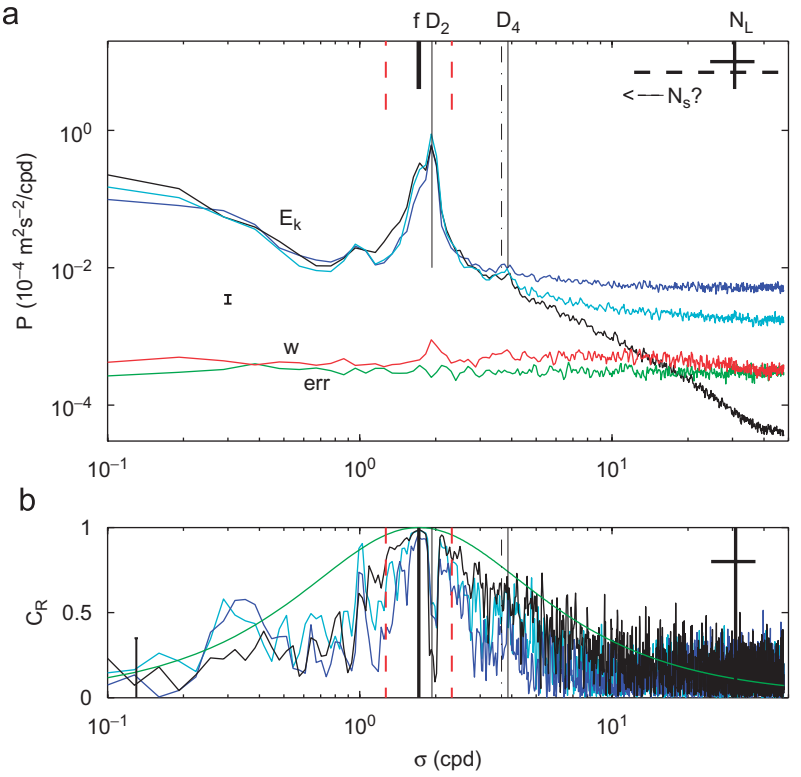

Fig. 5. (a) Heavily smoothed spectra at $z=-1012$ m from ADCP data: horizontal kinetic energy (E_k, blue), vertical velocity (w, red) and error velocity (err, green). For reference, E_k-spectra from $z=-872$ m (ADCP; light-blue) and from $z=-1005$ m (nearby moored current meter; black). (b) Moderately smoothed horizontal current polarization coefficient $C_R=2e/(1+e^2)$ ($=1$ for pure circular motions; $=0$ for rectilinear motions) using the same colors as in a. In green a linear wave model $C_R=2\sigma f/(\sigma^2+f^2)$ is given (Gonella, 1972). The red dashed lines indicate $\sigma=0.74$ and $1.35f$, whereas the horizontal black line indicates the $N_L\pm1$ std range due to variations with time. Thin solid lines indicate frequencies M_2 and M_4, the dash-dotted line M_2+f.

a familiar asymmetric polarization around f (Gonella, 1972), albeit not immediately dropping off for $\sigma<f$ as in other ocean areas (e.g., van Haren, 2004). It is noted, however, that here the ADCP's polarization varies at f, as do E_k and polarization asymmetry as a function of depth. This is due to variations in s/n.

The relatively large instrumental noise in u, v data (Table 1) directly affects the noise floor in **S**. The latter cannot be estimated better than within $\pm5\times10^{-3}\,s^{-1}$ per sample for $\Delta z=8$ m. As a result, the expected error for f, D_2 shear from hourly data is approximately $\pm4\times10^{-4}\,s^{-1}$.

Although horizontal motions are not so well resolved by the ADCP, its w data have a relatively lower noise level because of the acute beam angle ($\theta=20^\circ$) to the vertical. Thus, in the w-spectrum higher-frequency internal waves are still discernable for $\sigma>\sim7$ cpd. To further evaluate their quality, the w data are compared with the error velocity ('err') spectrum. Here, err is defined as a difference involving subtraction of the sum of beam pair velocities, instead of its mean as in w,

$$w=-\sum_{i=1}^{4} b_i/4\cos\theta,$$

$$\mathrm{err}=\sum_{i=1}^{2} b_i/4\cos\theta-\sum_{i=3}^{4} b_i/4\cos\theta,$$

where b_i denote the velocities in the directions of the four beams. The typical w-spectrum just significantly extends above err for most frequencies up to its roll-off frequency at $\sim N_L$, the same frequency at which Valeport's E_k is observed to roll off (Fig. 5a). Furthermore, w shows a significant peak at D_2, although the amplitude is small ($w_{D2}\approx10^{-3}\,m\,s^{-1}$).

The $\theta=20^\circ$ slant angle beams cause the ADCP to average current estimates over horizontal distances between 17 and 460 m. As a result, shear

estimates over finite vertical distances are biased low because of the horizontal separation of the beams. Alford and Pinkel (2000) estimated a most pessimistic case of 60% of the 'real' value for 6.4 m shear using a $\theta = 30^\circ$ slant angle ADCP. It is expected that in the present data, with a twofold larger range but smaller θ, this percentage represents the worst scenario as well. Alford and Pinkel also consider instrumental noise, which biases shear estimates high, as will be noticeable in the present data as well.

4. Observations

Short bursts of enhanced current amplitudes as well as relatively short vertical length scales are visible in Fig. 4b. Ridges of enhanced $|\mathbf{u}|$ are observed slightly slanted in z, t across most of the ADCP's range, with small variations in amplitude along such ridges. Although some (sub-inertial, inertial, semidiurnal tidal) periodicity can be determined from the raw $|\mathbf{u}|$ time series, periodic signals in shear computed from the raw data over the shortest possible vertical distance ($\Delta z = 8$ m) are difficult to distinguish from 'noise' time series (not shown).

However, a yearlong spectral mean demonstrates that shear over this $\Delta z = 8$ m is still dominated at frequencies in a combined f–D_2 band (Fig. 6), which just significantly stands out of the background white noise and which is larger than low-frequency shear that is fully biased high by the noise. The observed noise level is very close to the instrumental noise level estimated above. This explains the white character of the noise, which is not due to apparent Doppler shifting (see Section 5). The largest value in this f–D_2 band is found near f, not at D_2 frequencies. In fact, a relative gap down to the noise level is found at M_2. As $E_k(M_2)$ is more than half a decade larger than $E_k(f)$, this implies a relatively large dominant vertical scale at M_2. This is further evidence of dominant barotropic or coherent baroclinic tidal motions, although not at other D_2 frequencies like S_2. Motions at the latter seem to have a different source as they are largely incoherent. Only when $\Delta z > \sim 150$ m do vertical current differences at M_2 become larger than the otherwise rather flat f–D_2 'shear' band (Fig. 6). However, such vertical separation is not an appropriate measure for shear variance, which drops below a value of 0.1 times the value of $\Delta z = 8$ m f–D_2 shear for $\Delta z > 120$ m.

The spectral detail of $\Delta z = 24$ m shear (Fig. 7) shows some variation with depth, with most (near-inertial) shear being observed in the middle of the ADCP range, which corresponds to the shape of the mean shear profile (Fig. 3). It further shows peaks at S_2 at some depths and an apparent gradual broad-

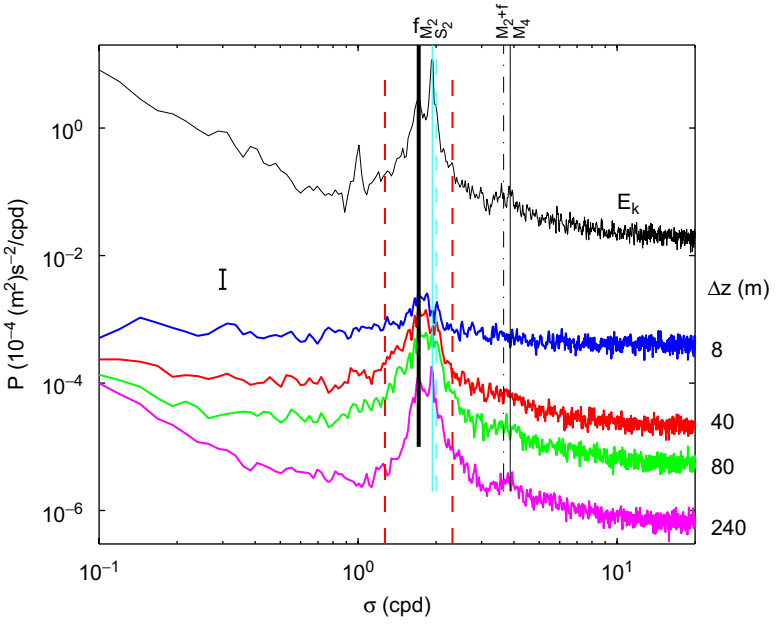

Fig. 6. Spectra of ADCP shear (in color; not offset arbitrarily) around $z \sim -710$ m for different vertical intervals. The arbitrarily offset kinetic energy spectrum (black) is shown for reference.

ening of the high-shear band with increasing amplitude, up to a bandwidth of ~0.75, 1.35f (with bounds at ~0.1$|\mathbf{S}|_{max}$) (Fig. 7). A relatively large portion, 30–40% of the total $f-D_2$ shear amplitude, is found at $\sigma<f$.

To further investigate the dominant inertial-tidal shear the f, D_2 bands are separated from the remainder of the signal using two sharp elliptic band-pass filters, extracting the bands 0.85–1.07f and 0.94–1.11M_2. The filters are used back and forth, so that phase is preserved. The upper inertial and lower tidal bounds are just separated ($1.07f \approx 0.94M_2$), while the other bounds assure a relative bandwidth $\Delta\sigma/\sigma > 0.1$ to capture more than 90% of f and D_2 variance. The sum of the two signals captures >99% of the variance in the combined band, whereas the relative error amounts to ~30%.

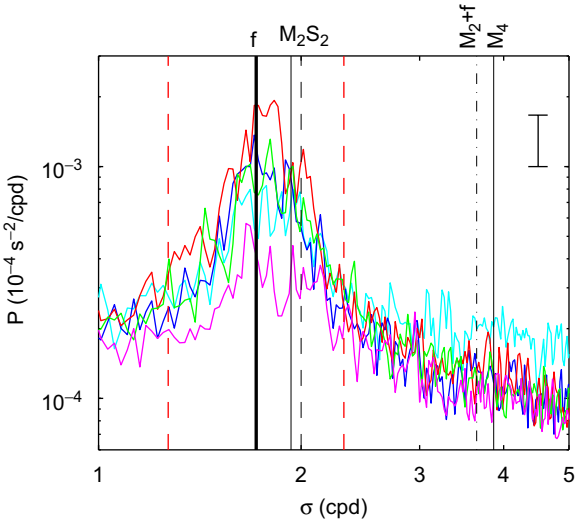

Fig. 7. Detail of $\Delta z = 24$ m shear spectra for $z = -988$ (light blue), −860 (dark blue), −724 (red), −588 (green) and −452 m (purple). The vertical lines indicate frequencies 0.74f (red dashed), f, M_2, S_2 (dashed), 1.35f (red dashed), besides inertial-tidal higher harmonics.

The filtered $\Delta z = 8$ m shear data (Fig. 8) demonstrate a much higher variability in the depth-time domain than the raw current data, implying that the shear magnitude is not dominated by the low-frequency (~monthly) periodicity (Fig. 4). Apparently, also the weakly z, t slanted $f-D_2$ currents (Fig. 4b) induce $|\mathbf{S}|$ across much smaller vertical and temporal scales. In time, the shear still reflects the familiar 'intermittency' or quasi-random variation of a few days in periodicity with time that is typical for incoherent internal waves. New is the image (Fig. 8) showing high variability in the vertical for the two different bands for a period of time as long as 1 year. In the vertical, shear shows maxima every 40 ± 15 m for both f and D_2. Amplitudes are up to $1.5 \pm 0.4 \times 10^{-4}\,s^{-1} \approx 12 \pm 3f$, and local maxima seem to concentrate near the center of the ADCP's range, between 600 and 800 m, for both frequency bands. This is approximately the same range for

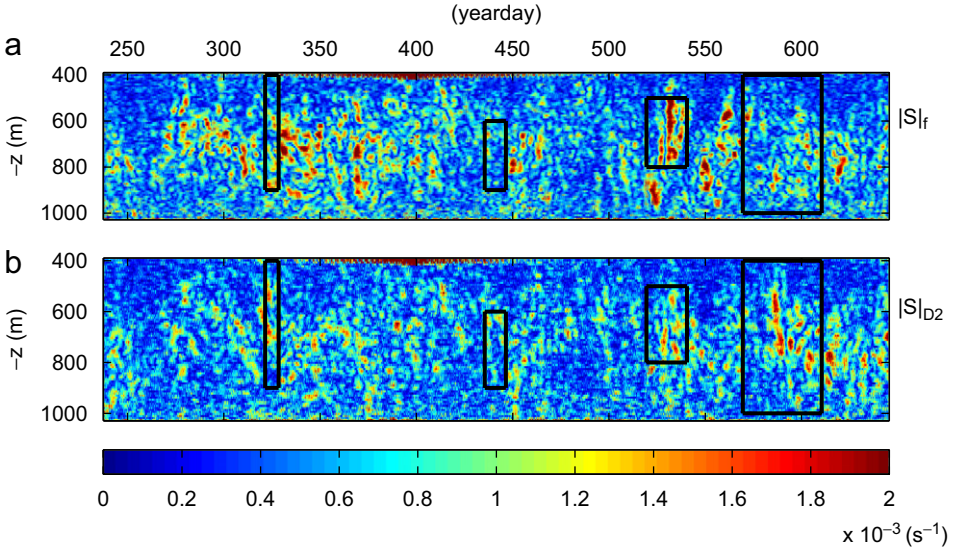

Fig. 8. Yearlong depth-time series of band-pass filtered shear ($\Delta z = 8$ m). Rectangles refer to periods in Fig. 9: (a) Near-inertial shear, (b) semidiurnal tidal shear.

increased $|\mathbf{u}|_f$, but it contrasts with the range of average enhanced $|\mathbf{u}|_{D2}$ that is found between 850 and 1000 m (van Haren, 2006).

The depth of maximum shear is very close to that of maximum N_L (computed from a single CTD profile; Fig. 3), which suggests that the large-scale stratification does not vary much over a year. It also suggests that N_L and $\langle|\mathbf{S}|\rangle$ are related as in a 'constant' *Ri*, as for example observed in the stratified North Sea (van Haren et al., 1999). Although the vertical profiles of N_L and $\langle|\mathbf{S}|\rangle$ are similar in shape, it may be obvious that these mean values do not yield a realistic indicator for diapycnal mixing as the 'mean' gradient Richardson number $N_L^2/\langle|\mathbf{S}|\rangle^2 \approx 5$. This is too large for instability to occur often. Not surprisingly, shear-induced mixing occurs over much smaller length and time scales than $\Delta z = 300$ m (used in N_L) and 1 year (used in $\langle|\mathbf{S}|\rangle$), respectively. However, in the vertical at any given time the number of short vertical scale shear maxima is of the same order of magnitude, about half the total number, as 8 m N_s minima/maxima (Fig. 3).

The appropriate z, t scales, to the limitation of the sampling, may be inferred from a few examples of detailed plots of f, D_2 shear amplitude (Fig. 9). As in the overall shear plot (Fig. 8), the detailed plots in Fig. 9 show a periodicity of $T_S = 3 \pm 1$ days, very similar for near-inertial and semidiurnal tidal shear. To first order, this period is longer than inertial (T_f)

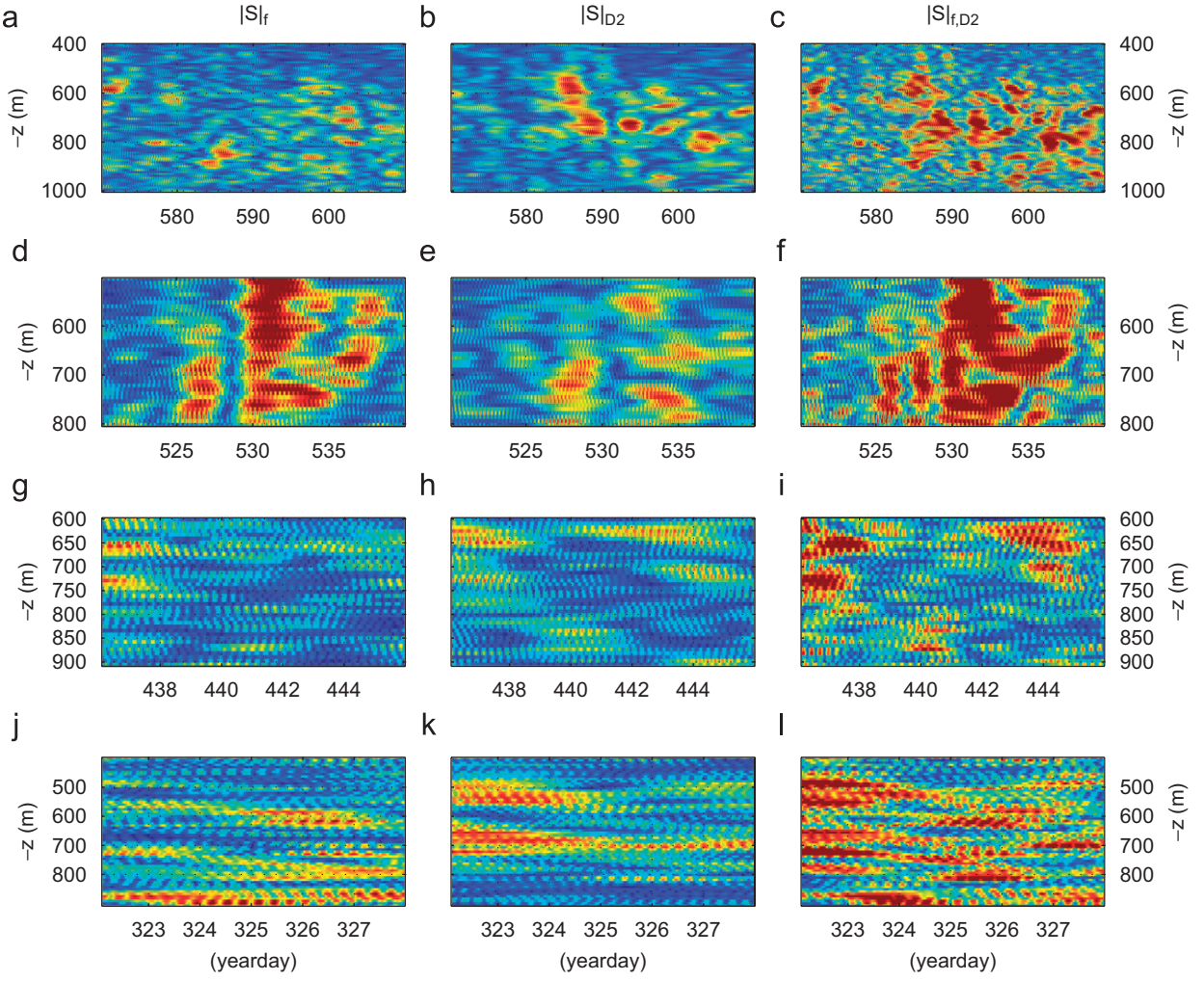

Fig. 9. Examples of depth time series of shear ($\Delta z = 8$ m). Colour coding is the same as in Fig. 8; note that vertical and horizontal scales vary between the periods. (a, d, g, j) Near-inertial shear. (b, e, h, k) Semidiurnal tidal shear. (c, f, i, l) Near inertial and semidiurnal tidal shear.

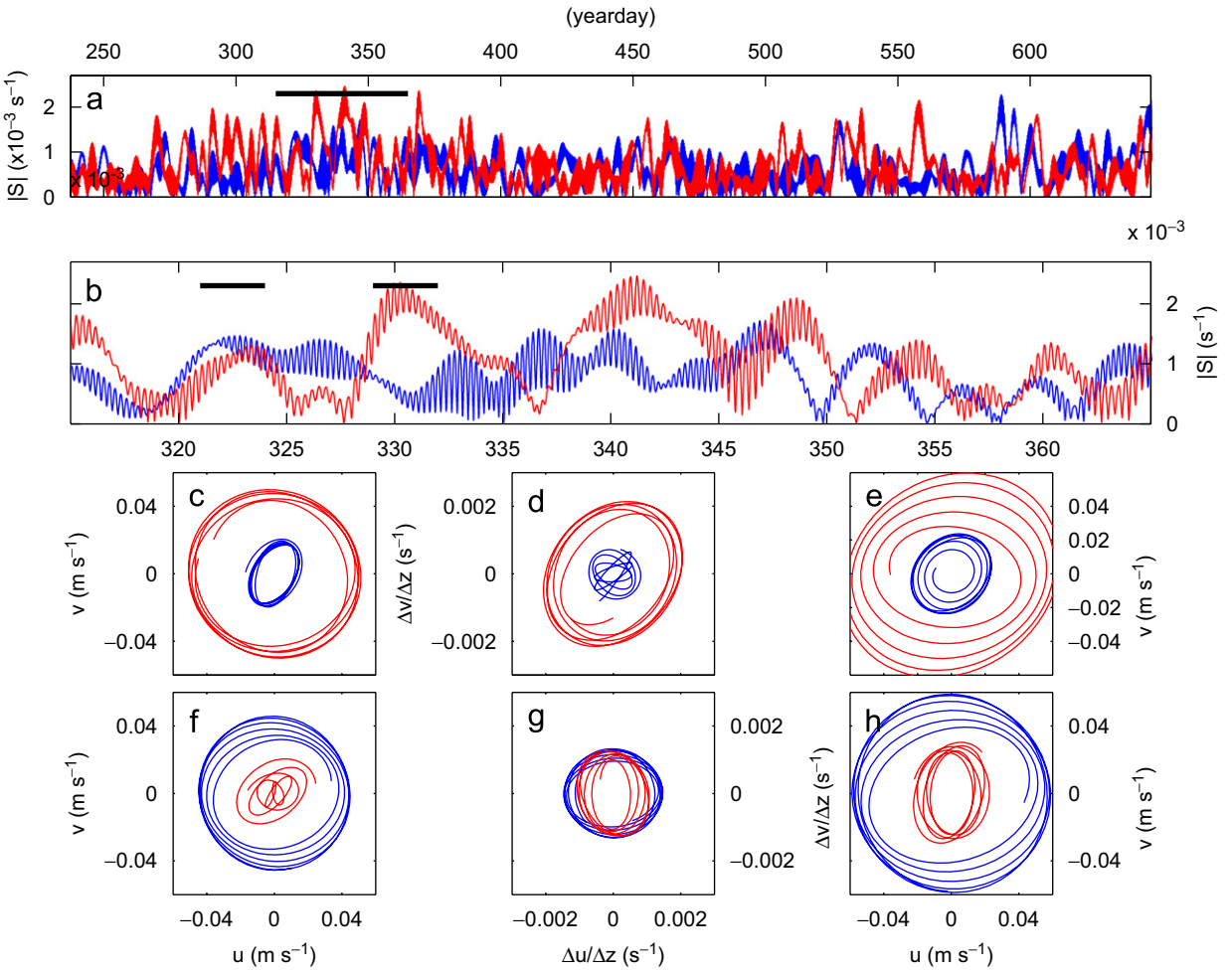

Fig. 10. Near-inertial (red) and semidiurnal tidal (blue) shear ($\Delta z = 8$ m) and currents near mid-depth. (a) Timeseries of shear around $z = -713$ m with the black bar indicating the period in (b). Detail of shear time series from a. with black bars indicating periods between days 321 and 324 (f–h); dominant tidal current) and between 329 and 332 ((c–e); dominant near-inertial current and shear). (c, f) Current ellipses at $z = -721$ m. (d, g) Shear ellipses around $z = -713$ m. (e, h) Current ellipses at $z = -705$ m.

and tidal (T_{D2}) periods, but shorter than the spring-neap cycle: $T_{D2} < T_f < T_S < T_{M2\text{–}S2}$. To second order, the T_f, T_{D2} periodicity can be seen superposed on T_S. This implies that shear is near-circular (Fig. 10), with an estimated $e = 0.8 \pm 0.2$. However, transitions and variations occur regularly, during which shear is commonly more rectilinear, albeit usually small.

In the vertical shear-*magnitude* planes are nearly horizontal, implying high vertical wavenumbers, with vertical length scales O(10–100 m) mentioned above: a flat pancake or sheet structure, in contrast to that of the current components (cf. Fig. 4b with Fig. 9g–i). The nearly horizontal $|\mathbf{S}|$ may be interpreted as near-circular shear with associated "slowly varying" magnitude, which can only be generated by circular motions (van Haren, 2000). Note that a combination of two counter-rotating circular motions of equal magnitude results in a rectilinear oscillatory motion, but such a motion can generate circular shear provided only one of the rotary components is sheared, as in Ekman dynamics across an internal boundary. Circular shear can result from the amplitude variations between the circular motions, but it will be enhanced when the phase of near-circular motions slants with depth.

Here, large differences are found between currents in neighboring depth-level bins (Fig. 10c, e, f, h note the near-equal f and D_2-shear while $|\mathbf{u}|_f \ll |\mathbf{u}|_{D2}$), with a tendency of the largest shear to be in the direction of the *minor* current ellipse axis.

Likewise, a tendency is observed of f-shear propagation being directed (along the minor axis) perpendicular to D_2-shear propagation (Fig. 10d, g), and, thus, of f-current propagation $\perp D_2$ currents. In general, peaks in $|\mathbf{S}|_f$ and $|\mathbf{S}|_{D2}$ seldom occur at the same time (Fig. 10a, b) and depth (Figs. 8 and 9). In terms of large-scale internal tidal topography and inertial atmospheric disturbance sources there is no plausible reason why $f \perp D_2$. A small-scale local interaction is suggested below.

5. Discussion

In shallow seas like the North Sea a nearly rectilinear, barotropic semidiurnal tidal current ($e<0.2$) can generate near-circular shear ($e>0.9$), because this shear is generated exclusively via the anti-cyclonic rotary (circular) component, to first order governed by viscous Ekman dynamics. There, the shear is maximal in the direction of minor current ellipse axis (van Haren, 2000). Open ocean shear from baroclinic currents observed here shows the same feature: to first order the shear's $e \sim 0.8$, with the major axis of shear directed along the minor ellipse axis of the current. This implies that maximum shear is in the direction of internal wave propagation, which is along the minor axis of currents. Inertial and tidal shear show the same behavior, but they do not seem to occur at the same depth at the same time. However, the second-order shear effects are still poorly explained, especially the effects during transition between large near-circular shear periods when the shear becomes much more rectilinear. How can a basically near-circular motion yield rectilinear shear?

In the present data, it must be the second-order deviation from circular motion that governs such rectilinear shear: the axis rotation of the slightly non-circular current ellipses. Assuming free propagating internal waves dominating f, D_2-motions, such rotation can be a manifestation of the wobbling in space-time of internal wave beams of which the angle to the vertical depends on N, σ, $f/\tan\varphi$ and $f_{\mathrm{eff}} = f + 0.5\zeta$. Here, ζ denotes the low-frequency (sub-inertial) vorticity, which is caused by a large-scale motion and which varies in value between 0.01 and $1f$ (Mooers, 1975; Kunze, 1985; van Haren, 2004). For example, for a wave of which propagation in the horizontal remains constant, a change in current ellipticity is induced by any vertical variation in N or f_{eff}, for fixed σ, ζ, φ and wave phase. This is because the internal wave

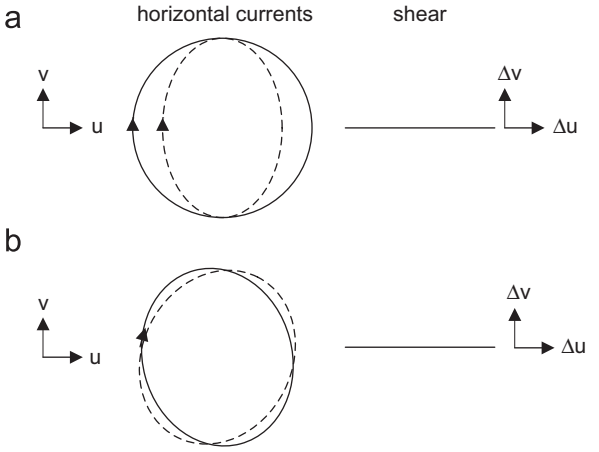

Fig. 11. Sketch of hypothetical generation of near-rectilinear shear from near-circular currents. (a) Variation in current ellipticity, e.g. due to variation in $N(z)$, so that propagation direction varies in the vertical. (b) Variation in horizontal propagation direction (ellipse inclination), e.g., due to refraction.

frequency bounds change relative to wave frequency, and hence ellipticity changes according to Gonella's (1972) model (see, Fig. 5). It is easily verified that this yields a rectilinear shear of which the major axis is directed along the minor axis of the current ellipse axis, the wave propagation direction (Fig. 11a). Likewise, a change in horizontal propagation direction creates rectilinear shear in the mean propagation direction, for fixed N, σ, ζ, φ and wave phase (Fig. 11b). Such change may be caused by refraction near a caustic or topography, or be evidence of a varying source, whereas the former model is associated with vertical variation in stratification: the layering in N_s.

From the large variations in N_s such layering can imply internal wave propagation and trapping at frequencies beyond internal gravity wave frequency bounds, for which the horizontal component of the Coriolis force $f/\tan\varphi$ needs to be considered (LeBlond and Mysak, 1978; Gerkema and Shrira, 2005). In this 'non-traditional approach' the internal inertio-gravity wave (IGW) band is broadened to $\sigma_{\min}(N,\varphi) < f < \sigma < \sigma_{\max}(N,\varphi)$, with $\sigma_{\min} \uparrow f$ and $\sigma_{\max} \downarrow N$ for $N \gg f$. Hence, this implies a further tilting of current ellipses for finite N. Recently, it has been observed that only waves in the IGW band between $0.74f < \sigma < 1.35f$, or equivalently $\sigma_{\min}(N \approx f) < \sigma < \sigma_{\max}(N \approx f)$ show asymmetric vertical phase propagation attributed to wave trapping in homogeneous ($N \leqslant f$, for $\sigma > f$) or stratified ($N \geqslant f$, for $\sigma < f$) layers (van Haren, 2006). The latter may

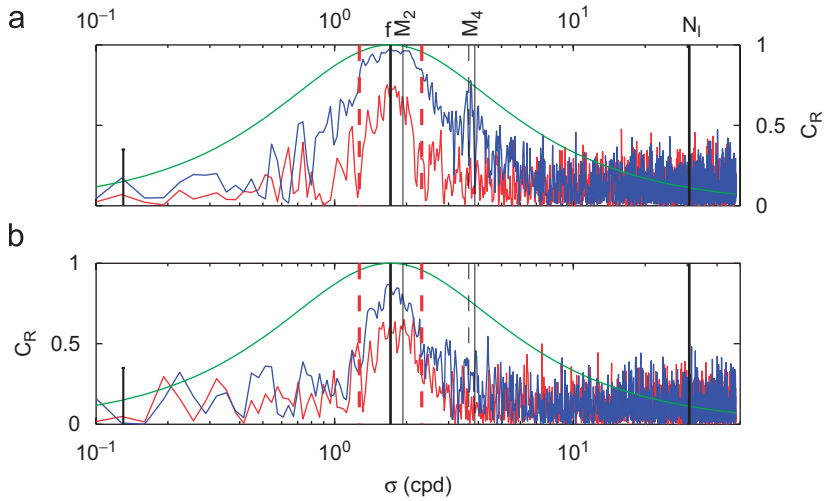

Fig. 12. Polarization coefficient as in Fig. 4b, but for yearlong shear. (a) Around $z=-713$ m using $\Delta z=8$ m (red) and 80 m (blue). (b) Using $\Delta z=16$ m around $z=-713$ m (blue) and $z=-465$ m (red). The vertical red dashed lines indicate $\sigma=0.74f$, $1.35f$, while the thin dashed line indicates M_2+f.

constitute the small-scale 'sheet internal waves' mentioned by Woods (1980).

As this IGW band contains sub-f, super-f and D_2, the sub-inertial part of the near-inertial motions is separated from the rest. This may explain the different shear layers observed here, as well as the flat shear band between the above frequency bounds and the near-complete symmetry in shear polarization around f (Fig. 12). In terms of a simple linear model, the latter implies symmetric rotary component forcing (Gonella, 1972), or forcing in a single Cartesian direction only, for which both $\sigma>f$ and $\sigma<f$ propagate freely. As both f *and* D_2 are contained in one IGW band of incoherent motions as suggested above, the model sketches in Fig. 11 may explain their interaction in terms of perpendicular propagation planes. However, this requires a frequency modulation (from f to D_2, and vice versa), which is not well understood. If so, this implies a local generation rather than large-scale sources.

The above band limited, flat and near-symmetric $f-D_2$ shear observations are not found exclusively at high latitudes where f is close to D_2. Symmetric shear polarization observations have also been made in the deep Canary Basin (van Haren, 2004), and flat-band $f-D_2$ is observed in Bay of Biscay ADCP data, except very near the continental slope internal tide source. In both areas, the current polarization is more asymmetric than observed here. A possible explanation for this symmetry contrast between current and shear polarization is suggested at the end of this section.

The approximate similarity for f and D_2 shear, and associated threefold smaller vertical length scale for f-motions compared to D_2, suggests similar internal wave behavior even in areas where f-motions are weak (in the Arctic under ice, possibly) and in areas where D_2 is small (Mediterranean Sea). This awaits further research. The f and D_2 shear cannot be studied strictly separately using the present data, not even in a strict isotherm-following coordinate system, because homogeneous and stratified layers are not very long lived (typically a few days, e.g., Marmorino et al., 1987, very likely related to internal wave straining), and because the present ADCP sampling smears very thin layers $\Delta z<20$ m and thus partially combines sub- and super-inertial shear. It is therefore not very relevant to study sub-f and super-f (including D_2), instead of f and D_2: the results are not very different (not shown), implying that f shear is dominated largely by *sub-inertial* motions, as anticipated.

Despite these shortcomings of the ADCP data and despite the lack of simultaneous yearlong N data over the ADCP range, which obstructs analysis in semi-Lagrangean isotherm-following coordinates, the observed Eulerian shear is not predominantly caused by vertical advection, awkwardly termed Doppler shifting, as in Sherman and Pinkel (1991). Firstly, the present study is limited to the $f-D_2$ band, which provides dominant motions or possible

sources, not subjects, for advection. Shear at other frequencies affected by advection is not considered here. Shear at those frequencies outside the f, D_2-band is dominated by instrumental noise. It is not caused by Doppler shift, which requires the larger-scale currents to be the source of the waves generating such shear. Secondly, w shows a small peak only at D_2, not at f. Thirdly, one may question the linearity of interacting IG waves. Fourthly, as is visible in the time domain in observations by Alford and Pinkel (2000) and as is demonstrated in the frequency domain by van Haren (2000), the long-term average spectra of properly resolved Eulerian and semi-Lagrangean shear from ADCP data do not differ substantially, especially not in the $f-D_2$ band.

The strict partition in space and time between f and D_2 shear can also be understood from the following Ri-argumentation, which holds for any shear generated by motions at two different frequencies, not just f and D_2. Suppose an internal D_2-wave propagates through an f-shear field. Then D_2 shear associated with the propagating wave can develop only where the existing f shear is low and N relatively high ($Ri>1$). Otherwise, in a layer of high $|\mathbf{S}|_f$, low N and marginal $Ri<1$, the additional D_2 shear will generate instability that destroys the wave. Thus, large f and D_2 shear must be separated. Similarly, a wave beam that passes through varying stratification and vorticity background may generate instabilities below the marginal stability level $Ri\sim0.25$–1, or it can exist only in layers where shear is (still) relatively weak ($Ri>1$).

The sum of f and D_2 shear (and shear at other frequencies, if important) is related to regions of high N (Pinkel and Anderson, 1997), while locally $Ri<1$ still, or a marginal stable state. This is predicted for low-mode internal waves (Phillips, 1966) and found in the North Sea, where typically $\Delta z=1$ m and f, D_2 are mainly barotropic (van Haren et al., 1999). It is also found here (Fig. 13) and, although ADCP time series and individual CTD profiles cannot be matched precisely, the comparison is striking using similar scales ($\Delta z\approx25$ m). Hypothetical $Ri\sim1$ regularly, even without taking into account the possible low bias of the $|\mathbf{S}|$-estimates down to 60% because of the ADCP's beam spread. However, the present ADCP data are probably too limited to detect the shear roll off in the ocean (cf. Fig. 3) for the smaller scale N variations.

The observation of high variability of near inertial and tidal shear in the z, t plane questions

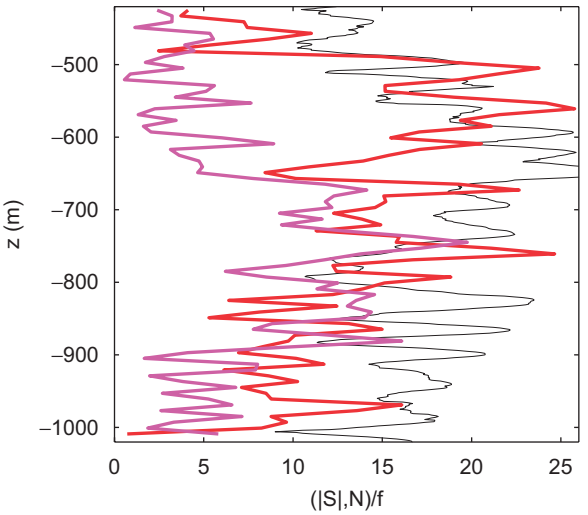

Fig. 13. Stratification computed from CTD data over $\Delta p=25$ dbar (thin black). In red (day 530.5) and purple (day 310) individual near inertial and semidiurnal tidal shear profiles ($\Delta z=8$ m). Shear is not corrected for beam spread and noise. In the worst case, the presented $|\mathbf{S}|$ values should be multiplied by a factor of 1.6.

the generation of such layering, far from the influence of external frictional boundaries near the surface and bottom. Rainville and Pinkel (2004) attribute shear layering to internal wave propagation, as bands of layers tend to slope to internal wave rays 'in a quiescent background'. The latter implies computation of wave ray slopes using smooth N, as is common practice. However, this does not comply with the associated local enhanced shear and the likewise strained internal wave field that generates high N locally, which can act as a local 'smooth' high N environment for short-scale waves. Furthermore, the suggested large-scale N_L for internal wave propagation does not hold for large-scale areas where $N=0$, as in the western Mediterranean Sea (van Haren and Millot, 2004). Hence, a better model for internal wave propagation is needed, a model that accounts for local N and for the effects of shear from different (tidal, inertial) sources affecting other wave frequencies, and also each other.

The small-scale N_s layering so ubiquitous in the ocean (e.g., Marmorino et al., 1987; Alford and Pinkel, 2000; Nandi et al., 2004; Holbrook and Fer, 2005; present data) may be caused by non-internal-wave processes like double-diffusive mixing that have typical scales of O(1–100 m) for homogeneous layers, but also seems to occur in non-double diffusion favorable areas. The layering may

therefore equally well be generated by internal waves. Internal wave straining following non-linear interactions from one or more primary waves will cause periodic layering of the stratification. More permanent N variation is caused by localized convective overturning occurring for the wave when particle velocity $u > c$, the phase speed (Orlanski and Bryan, 1969), or breaking of non-linearly generated higher harmonics at the f, D_2-shear. A typical vertical length scale associated with the former is $O(10\,\mathrm{m})$, depending on N, whereas horizontal scales are $O(10^2$–$10^5\,\mathrm{m})$. These "pancake" areas of homogeneous water may adjust geostrophically, generating vortical modes (low frequency non-propagating motions), which may interact with internal waves (Lelong and Riley, 1991).

Although Polzin et al. (2003) demonstrate that such vortical modes are generally much less energetic than other motions like internal waves, possibly only contributing to the E_k-spectrum in the narrow sub-f frequency band between $0.2 < \sigma < 0.6$–1 cpd, they may explain the polarization contrast between currents (asymmetric around f, Gonella, 1972; van Haren, 2004) and shear (symmetric around f, present data). Here, the non-propagating motions seem to contribute little to shear while dominating E_k over sub-inertial IG-waves close to the low-frequency limit, for $N = f$. This confirms Canary Basin observations by Polzin et al. (2003), demonstrating that internal wave shear dominates vortical mode shear. However, Polzin et al. (2003) also demonstrate that the latter shear dominates the short ($\sim$10 m) vertical scales, which seems at odds with the present findings, as f–D_2 shear is largest at the shortest scales. It also remains to be established whether vortical modes dominate the f–D_2 interaction and shear beat periods of $\sim$2 days, while current (not shear) polarization peaks are observed at frequencies 0.2–0.3 cpd (Fig. 5b; recall that the f–M_2 beat period is 4.5 days and f–S_2 3.4 days).

Future investigations of further yearlong observations are needed of consecutive N, $|\mathbf{S}|$ at smaller vertical scales, down to 1 m preferably, to solve some of these remaining issues. Likewise, one may question the use of mean stratification to stretch the vertical coordinate, by scaling with $N^{1/2}$, to obtain a WKB smooth ocean. Variations in the z, t plane seem too rapid, even on f, D_2 scales. As mentioned by Pinkel (1983), WKB depth stretching distorts the simple patterns of vertical phase propagation that were apparent in his unstretched data.

Acknowledgments

I thank the crews of the R./V. *Pelagia* (deployment) and R./V. *Darwin* (recovery) and Hendrik van Aken for the logistics operation of obtaining the data. Theo Hillebrand prepared the mooring and instrumentation. Margriet Hiehle provided Fig. 1. The comments of the anonymous referees are highly appreciated. Most of the data analysis and preparation of the manuscript were done during a stay at Ifremer, La Seyne-sur-mer, France. I thank Claude Millot for discussions and comments. Our French–Dutch collaboration is supported by the Netherlands Organizsation for the Advancement of Scientific Research, NWO, and Centre Nationale de la Recherche Scientifique, CNRS. LOCO is supported by a large-budget investment Grant from NWO.

References

Abarbanel, H.D.I., Holm, D.D., Marsden, J.E., Ratiu, T., 1984. Richardson number criterion for the nonlinear stability of three-dimensional stratified flow. Physical Review Letters 52, 2352–2355.

Alford, M.H., Pinkel, R., 2000. Observations of overturning in the thermocline: the context of ocean mixing. Journal of Physical Oceanography 30, 805–832.

Baines, P.G., 1982. On internal tide generation models. Deep-Sea Research 29, 307–338.

Davies, A.M., Xing, J., 2003. On the interaction between internal tides and wind-induced near-inertial currents at the shelf edge. Journal of Geophysical Research 108 (C3), 3099.

Davies, A.M., Xing, J., 2005. The effect of a bottom shelf front upon the generation and propagation of near-inertial internal waves in the coastal ocean. Journal of Physical Oceanography 35, 976–990.

Fu, L.-L., 1981. Observations and models of inertial waves in the deep ocean. Review of Geophysics and Space Physics 19, 141–170.

Gargett, A.E., Hendricks, P.J., Sanford, T.B., Osborn, T.R., Williams III, A.J., 1981. A composite spectrum of vertical shear in the upper ocean. Journal of Physical Oceanography 11, 1258–1271.

Garrett, C.J.R., Munk, W.H., 1972. Space-time scales of internal waves. Geophysical Fluid Dynamics 3, 225–264.

Gerkema, T., Shrira, V.I., 2005. Near-inertial waves in the ocean: beyond the "traditional approximation". Journal of Fluid Mechanics 529, 195–219.

Gonella, J., 1972. A rotary-component method for analysing meteorological and oceanographic vector time series. Deep-Sea Research 19, 833–846.

Gregg, M.C., 1989. Scaling turbulent dissipation in the thermocline. Journal of Geophysical Research 94, 9686–9698.

Holbrook, W.S., Fer, I., 2005. Ocean internal wave spectra inferred from seismic reflection transects. Geophysical Research Letters 32, L15604.

Kunze, E., 1985. Near-inertial wave propagation in geostrophic shear. Journal of Physical Oceanography 15, 544–565.

Leaman, K.D., 1976. Observations on the vertical polarization and energy flux of near-inertial waves. Journal of Physical Oceanography 6, 894–908.

Leaman, K.D., Sanford, T.B., 1975. Vertical propagation of inertial waves: a vector spectral analysis of velocity profiles. Journal of Geophysical Research 80, 1975–1978.

LeBlond, P.H., Mysak, L.A., 1978. Waves in the Ocean. Elsevier, Amsterdam.

Lelong, M.-P., Riley, J.J., 1991. Internal wave-vortical mode interactions in strongly stratified flows. Journal of Fluid Mechanics 232, 1–19.

Marmorino, G.O., Rosenblum, L.J., Trump, C.L., 1987. Fine-scale temperature variability: the influence of near-inertial waves. Journal of Geophysical Research 92, 13049–13062.

Mooers, C.N.K., 1975. Several effects of a baroclinic current on the cross-stream propagation of inertial-internal waves. Geophysical Fluid Dynamics 6, 245–275.

Nandi, P., Holbrook, W.S., Pearse, S., Páramo, P., Schmitt, R.W., 2004. Seismic reflection imaging of water mass boundaries in the Norwegian Sea. Geophysical Research Letters 31, L23311.

Orlanski, I., Bryan, K., 1969. Formation of the themocline step structure by large-amplitude internal gravity waves. Journal of Geophysical Research 74, 6975–6983.

Phillips, O.M., 1966. The Dynamics of the Upper Ocean. Cambridge University Press.

Pinkel, R., 1983. Doppler sonar observations of internal waves: wave-field structure. Journal of Physical Oceanography 13, 804–815.

Pinkel, R., Anderson, S., 1997. Shear, strain, and Richardson number variations in the thermocline. Part I: statistical description. Journal of Physical Oceanography 27, 264–281.

Polzin, K.L., Toole, J.M., Ledwell, J.R., Schmitt, R.W., 1997. Spatial variability of turbulent mixing in the abyssal ocean. Science 276, 93–96.

Polzin, K.L., Kunze, E., Toole, J.M., Schmitt, R.W., 2003. The partition of finescale energy into internal waves and subinertial motions. Journal of Physical Oceanography 33, 234–248.

Rainville, L., Pinkel, R., 2004. Observations of energetic high-wavenumber internal waves in the Kuroshio. Journal of Physical Oceanography 34, 1495–1505.

Sherman, J.T., Pinkel, R., 1991. Estimates of the vertical wavenumber-frequency spectra of vertical shear and strain. Journal of Physical Oceanography 21, 292–303.

St. Laurent, L., Garrett, C., 2002. The role of internal tides in mixing the deep ocean. Journal of Physical Oceanography 32, 2882–2899.

Turner, J.S., 1973. Buoyancy Effects in Fluids. Cambridge University Press.

van Haren, H., 2000. Properties of vertical current shear across stratification in the North Sea. Journal of Marine Research 58, 465–491.

van Haren, H., 2004. Spatial variability of deep-ocean motions above an abyssal plain. Journal of Geophysical Research 109, C12014.

van Haren, H., 2006. Asymmetric vertical internal wave propagation. Geophysical Research Letters 33, L06618.

van Haren, H., Maas, L., Zimmerman, J.T.F., Ridderinkhof, H., Malschaert, H., 1999. Strong inertial currents and marginal internal wave stability in the central North Sea. Geophysical Research Letters 26, 2993–2996.

van Haren, H., Millot, C., 2004. Rectilinear and circular inertial motions in the Western Mediterranean Sea. Deep-Sea Research I 51, 1441–1455.

Walter, M., Mertens, C., Rhein, M., 2005. Mixing estimates from a large-scale hydrographic survey in the North Atlantic. Geophysical Research Letters 32, L13605.

Woods, J.D., 1980. Do waves limit turbulent diffusion in the ocean? Nature 288, 219–224.